Interface Dipoles Arising from Self-Assembled Monolayers on Gold: UV−Photoemission Studies of Alkanethiols and Partially Fluorinated Alkanethiols

Dana M. Alloway,[†] Michael Hofmann,[†,§] Darrin L. Smith,[†] Nadine E. Gruhn,[†] Amy L. Graham,[†] Ramon Colorado, Jr.,[‡] Vicki H. Wysocki,*[,†] T. Randall Lee,*[,‡] Paul A. Lee,[†] and Neal R. Armstrong*[,†]

Department of Chemistry, University of Arizona, Tucson, Arizona 85721, Department of Chemistry, University of Houston, Houston, Texas 77204-5003, and Institut für Angewandte Photophysik (IAPP), Technische Universität Dresden, Dresden, Germany

Received: March 14, 2003; In Final Form: August 7, 2003

Gold surfaces modified with C_3-C_{18}-alkanethiols ($CH_3(CH_2)_{X-1}SH$; H_XSH; $x = 3, 8, 12, 16, 18$) and C_{16}-alkanethiols, fluorinated at the outer 1, 2, 4, and 10 methylene positions ($CF_3(CF_2)_{Y-1}(CH_2)_XSH$; F_yH_xSH; $y = 1$, $x = 15$; $y = 2$, $x = 14$; $y = 4$, $x = 12$; $y = 10$, $x = 6$) were characterized by He(I) UV-photoelectron spectroscopy (UPS). (Detailed X-ray photoelectron spectroscopic characterization of the partially fluorinated thin films is given in the Supporting Information). Long incubation times of the gold surface with the alkanethiol solutions lead to compact monolayer films for all of the alkanethiols, as indicated by the exponential decrease in emission intensity versus alkyl chain length for both the gold Fermi edge (UPS data), and by a parallel decrease in Au(4f) photoemission intensity using X-ray photoelectron spectroscopy. Changes in the effective work function of these surfaces due to the presence of significant interfacial dipoles are observed (*i*) as alkyl chain length is increased, and (*ii*) as the fraction of fluorinated methylene groups is increased in a constant length alkyl chain. Negative shifts of the low kinetic energy photoemission edge with increasing alkyl chain length in the H_xSH series are consistent with the presence of a large positive interface dipole. The largest part of this shift (ca. 1.0 eV) appears between the C_3- and C_8-alkyl chain lengths. Adding $-CF_x$ groups to the outer end of the C_{16}-alkyl chain positively shifts the low-kinetic-energy photoemission edge, consistent with the presence of a large negative interface dipole that completely compensates for the positive dipole from the alkyl portion of the chain. Examining $C_{13}-C_{16}$ alkyl chains fluorinated at only the outer methyl group shows that this negative dipole depends on the orientation of the $-CF_3$ group (i.e., "odd−even" effects in the effective work function are observed). Comparison of the shifts in gold/SAM vacuum level (changes in effective work function) as a function of the apparent dipole moment of the molecule provides an estimate of the band-edge offsets for these molecules on the gold surface, an estimate of the intrinsic shift in a vacuum level at zero dipole moment of the adsorbate, and an estimate of the intrinsic dipole moment for the gold−thiolate bond.

Introduction

Chemical modification schemes are of interest to tailor the effective work function of both conductor (metal, metal oxide, and molecular/polymeric semiconductors) and nonconductor surfaces to control energetic barriers to charge injection.[1−19] Self-assembled monolayers (SAMs) of alkanethiols on metal or semiconductor surfaces are one approach to tailoring surface composition with close-packed molecules with variable terminal group composition, chain length, and film thickness. Ulman and Evans,[2] and Campbell et al.[3,4] showed changes in surface potential as either the length of the alkyl chain or the electron affinity of the terminal functional group is varied, while Sita and co-workers showed similar effects using arenethiols with different terminal functional groups.[5] Howell et al. recently extended these measurements to submicron dimensional scales using electrostatic force microscopy,[18] while Frisbie and co-workers have used conductive-tip AFM to characterize barrier heights and control of tunneling current with arenethiols on gold.[6−8] Cahen and co-workers have shown that the rectification properties of Au/organic and GaAs/organic contacts can be controlled by the addition of self-assembled monolayers, and demonstrated that the onset potentials for charge injection correlate well with the barriers created by surface modifiers with both positive and negative dipoles.[9−12] Similar studies using covalently bonded surface modifiers on metal and metal oxide surfaces suggest that a wide degree of control of effective surface work function is possible,[13−17]

These energetic barriers are also likely to be significant in controlling the extent of molecular ion fragmentation in a new form of mass spectrometry, known as surface-induced-dissociation (SID).[20,21] As the positive molecular ions of benzene ($C_6H_6^+$) and pyrazine ($C_4H_4N_2^+$) collide with an alkanethiol-modified metal surface neutralization of these incoming ions competes with other fragmentation pathways. Recent studies have shown that the neutralization probability appears to scale inversely with alkane chain length of the surface modifier and is strongly affected by the presence of high-electron-affinity substituents in the alkane chain. The barriers to injection of an

* Authors to whom correspondence should be addressed. E-mail (Armstrong): nra@u.arizona.edu. E-mail (Lee): trlee@uh.edu. E-mail (Wysocki): vwysocki@u.arizona.edu.
† University of Arizona.
‡ University of Houston.
§ Technische Universität Dresden.

10.1021/jp034665+ CCC: $25.00
Published on Web 09/25/2003

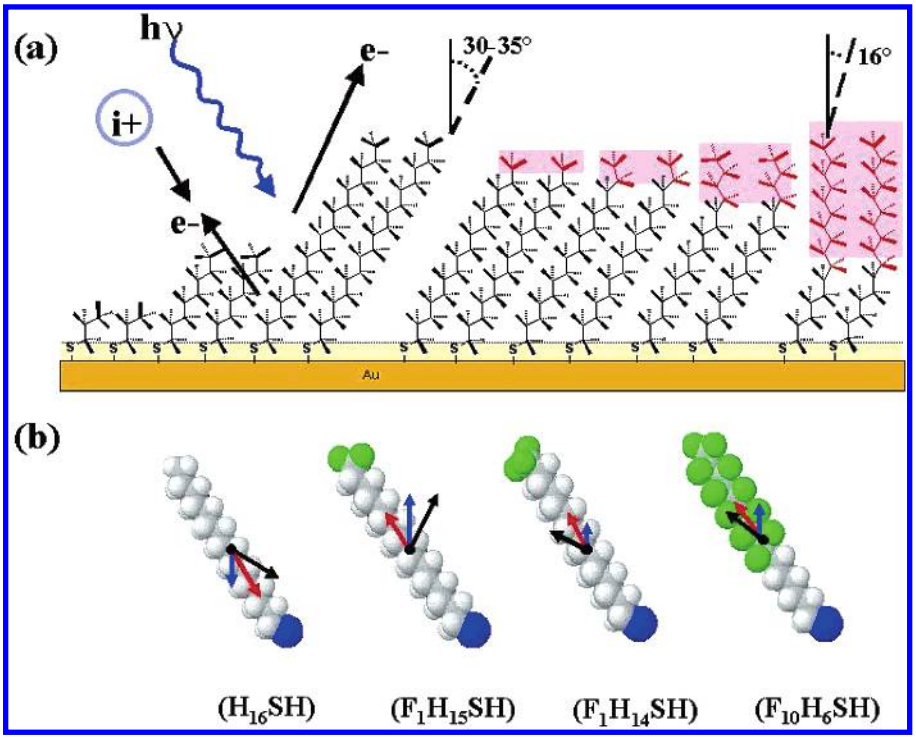

Figure 1. (a) Schematic view of normal alkanethiols (H_3SH, H_8SH, and $H_{18}SH$) and partially fluorinated 16-carbon alkanethiols (F_yH_xSH, y = 1,2,4,10) examined by UPS in this study. Approximate tilt angles are shown (refs 16−17,20−21); (b) schematic view of $H_{16}SH$ and selected partially fluorinated alkanethiols, indicating the vectoral direction and magnitude of the expected dipole moments: black arrows are for the total calculated dipole moments; red arrows (along molecule) are shown for dipoles along the molecular axis; and blue arrows represent the dipole normal to the surface.

electron from the substrate metal to an incoming ion (through the SAM layer) are likely to be strongly correlated with the barriers of importance for molecular electronic applications of these same thin films.

Kelvin-probe measurements, which can be conducted in both vacuum and atmosphere, and photoelectron spectroscopies have been used to estimate changes in effective work functions of metal and semiconductor surfaces as modifiers are added to these surfaces.[1−5,9−16,22−30] UV photoelectron spectroscopy (UPS) in high vacuum environments traditionally takes the total width of the photoemission spectrum, subtracted from the source energy, as an estimate of effective work function of clean metals and semiconductors. UPS and X-ray photoelectron spectroscopy (XPS) are also used to follow changes in effective work function induced by the formation of heterojunctions, charge exchange at interfaces, and charge redistribution effects that extend a few nanometers away from these interfaces.[22−30] In addition to traditional metal/semiconductor and semiconductor/semiconductor heterojunctions, these measurements have recently been applied to a series of vacuum-deposited organic layers on metals, metal oxides, and other semiconductors, and on organic/organic heterojunctions. When charge exchange occurs upon formation of heterojunctions, shifts in the vacuum level are observed, which can be as large as 1 eV and are attributed to interface dipole formation.[14,22−30] These effects are, in general, much larger for adsorption of organic layers on metal surfaces with large intrinsic electronic surface dipoles, and much smaller for organic/organic heterojunctions. The general rules in discussing work function changes, interface dipole effects, and the influence of these changes on device properties have been recently reviewed and restated by Cahen and Kahn.[24]

Duwez et al. recently reported the characterization of alkanethiols, alkanedithiols, and cyclopentyl- and cyclohexylalkanethiols adsorbed on gold surfaces using UV-photoemission spectroscopy to probe the structure and compact nature of these monolayer films.[31,32] No mention was made, however, of the apparent differences in interfacial dipoles that might arise from these different surface modifiers. Seki and co-workers have conducted similar studies on LB-deposited thin films, where shifts in a vacuum level *were* noted because of the addition of a close-packed alkane layer to a metal or semiconductor substrate.[33]

Recent vacuum-STM studies of H_xSH versus F_yH_xSH films on Au(111) surfaces by Pflaum et al. have shown that substituting just the terminal $-CH_3$ group with a $-CF_3$ group introduces a significant Coulombic energy barrier to charge injection, confirming that dipoles are expressed at both the metal/organic interface and at the organic/vacuum interface.[16] Surface wetting studies on similarly modified surfaces also suggest the presence of strong local surface dipoles, and Lee and co-workers have found that polar liquids wet CF_3-terminated SAMs on gold, derived from $CF_3(CH_2)_nSH$, markedly more than CH_3-terminated alkanethiols, derived from $CH_3(CH_2)_nSH$.[35−40] These enhanced wettabilities to polar liquids, however, decrease systematically as the degree of fluorination is further increased (i.e., with the use of $CF_3CF_2(CH_2)_{n-1}SH$ and more highly fluorinated alkanethiols).

We document here our recent studies of compact layers of both hydrocarbon and partially fluorinated alkanethiol monolayers on gold, as shown in Figure 1, with special attention paid to the shifts that occur in the photoemission spectrum at the low kinetic energy (KE) edge. As shown schematically in this figure, we assume that the alkanethiol chains terminated with a single $-CF_3$ group adopt essentially the same packing behavior as for the $-CH_3$ terminated chains ($-CH_3$ terminated chains have $(\sqrt{3} \times \sqrt{3})R30°$ structures with a ca. 5.0 Å lattice spacing, a tilt angle of 35° (relative to surface normal), and a β-twist angle of 55° (rotation around the molecular axis) (Figure 1).[1,16,41−44] As the fraction of $-CF_x$ groups on the alkyl chain is increased, the fluorinated sections are expected to adopt a

more upright orientation with respect to the surface normal (tilt angles of ca. 16° versus ca. 35°), occupying more space on the surface (forming p(2×2) or c(7×7) structures with an average intermolecular spacing of ca. 5.9 Å.[41] The abbreviated notations used in this paper for thiol monolayers are H_XSH for the molecular formula $CH_3(CH_2)_{X-1}SH$ and F_YH_XSH for the molecular formula $CF_3(CF_2)_{Y-1}(CH_2)_XSH$.

Shifts in low-KE edge (vacuum level) are observed from these data, but the majority of the effect is obtained with either the shortest chain length alkanethiols (positive interface dipoles) or with the minimum addition of fluorination to the C_{16}-alkyl chain (addition of a negative dipole). The positive dipole achieved by addition of the C_{16}-alkanethiol to the gold surface is compensated by the presence of electronegative fluorine groups, suggesting a convenient means of controlling the energy barrier to charge injection at such interfaces. Comparison of the shifts in a vacuum level induced by the addition of both the normal and partially fluorinated alkanes provides a means of estimation of the intrinsic shift in a vacuum level induced by an alkanethiol with zero effective dipole moment, and hence the intrinsic dipole moment in the gold−thiolate bond.

Experimental Section

Sample Preparation. Polycrystalline gold foil samples (area = 1 cm^2) were cleaned with a solution of micropolishing alumina, with 1.0 μm and 0.3 μm particle sizes, and rinsed in water and ethanol. These samples were then soaked in a sulfuric acid−hydrogen peroxide (30 %) mixture (ratio 4:1) for 15 min. After rinsing in ethanol and drying with purified nitrogen, the samples were inserted in an air plasma-cleaner (Harrick) for 15 min at 60 W power dissipation.

These gold samples were then immediately immersed in 1 mM ethanol solutions of either the alkanethiol or the partially fluorinated alkanethiol for 72 h. Normal alkanethiols were purchased from Aldrich and used without further purification. The fluorinated alkanethiols were synthesized using established procedures (F_YH_XSH and F_1H_XSH).[45] After emersion from the thiol solution, the SAM-modified gold foils were rinsed in ethanol, dried with nitrogen, and immediately loaded into the ultrahigh vacuum surface analysis chamber. Exposure to the atmosphere after modification typically occurred for less than one minute. XPS analysis of such samples, in the S(2p) region showed no detectable oxidation of the sulfur groups to form functional groups such as $-SO_3^-$.

UPS and XPS Measurements—Thin Films. All measurements were conducted in a combined UPS-XPS Kratos Axis Ultra with an average base pressure of 10^{-9} Torr. Several identical gold samples were examined in succession during each day of analysis so that all of the alkanethiol-modified gold surfaces or partially fluorinated alkanethiol-modified gold surfaces could be characterized with identical instrument parameters. XPS data were collected with monochromatic Al(Kα) radiation at a pass energy of 20 eV. UPS spectra were obtained with a 21.2 eV He (I) excitation (Omicron VUV Lamp HIS 13) and pass energy of 5 eV. For all UPS analyses, a 5 V bias was applied to improve the transmission of low KE electrons and to improve the determination of the energy of the low-KE edge.[22−30] Separate UPS spectra and XPS spectra were measured for a sputter-etched, atomically clean gold sample on each day of analysis before characterization of the SAM-modified samples to ensure that instrument parameters were the same as for all previous studies. This process ensured that the low-KE edge, relative intensities of the low and high kinetic energy peaks, and the intensity of photoemission at the Fermi edge relative to the lowest KE region were consistent for all samples. All spectral features for identically modified samples appeared at energies reproducible to within ±0.05 eV.

Previous investigations have suggested that alkanethiol-based SAMs are sensitive to X-ray-induced modification.[46,47] The X-ray source was therefore operated at only 150 W, sample exposure to X-rays was kept to a minimum (ca. 30 min or less), and all XPS data were collected *after* the UPS data were obtained to further minimize damage. UPS data recorded after XPS characterization, however, showed no discernible changes in frontier orbital photoemission, which might have arisen had decomposition occurred.

To ensure that these thin films retained their composition throughout their characterization, XPS data were collected for the partially fluorinated alkanethiol series on gold, before and after UPS analysis (A figure showing these XPS data appear at the end of this manuscript and is available as Supporting Information). The C(1s) XPS data for the same series of Au surfaces as in Figure 5 showed a monotonic decrease in photoemission intensity of the CH_x-like hydrocarbons (285.6−285.3 eV) and an increase in photoemission intensity of the CF_x-like hydrocarbons (291.5 eV) as the extent of fluorination increased. Changes in absolute peak areas, and the area ratio and relative atomic ratios (CF_x/CH_x), computed from these XPS data, all agreed with those expected from stoichiometric material and did not change with X-ray exposure time, demonstrating that the composition of the partially fluorinated films is consistent with previous characterizations of their composition and structure. In addition, no C(1s) XPS peaks were observed at binding energies between 286 and 291 eV, further confirming the stability of these partially fluorinated alkyl chains.[46]

UPS Measurements—Gas Phase. Gas-phase photoelectron spectroscopy was performed for several of the alkanethiols and partially fluorinated alkanethiols, using instruments and general experimental methods that have been described in detail previously.[48] The alkanethiol H_8SH is a liquid and was introduced into the spectrometer from a sealed glass tube with a sidearm attached to an internal stainless steel tube via a variable leak valve with no need for sample heating. Similarly, $H_{12}SH$ is also a liquid, and the data were collected with the sample in an internal aluminum sample cell that had been cooled to 10−18 °C. All other samples analyzed by gas-phase spectroscopy were solids, and the data were collected with the samples in the aluminum sample cell, which was heated to 40−85 °C depending on the volatility of the samples. The argon $^2P_{3/2}$ ionization at 15.759 eV was used as an internal calibration lock, and the difference between the argon $^2P_{3/2}$ ionization and the methyl iodide $^2E_{1/2}$ ionization at 9.538 eV was used to calibrate the ionization energy scale. The instrument resolution (measured by the full width at half-height of the $^2P_{3/2}$ ionization of Ar) during data collection was always better than 25 meV.

Results and Discussion

Characterization of Thin Film and Gas-Phase Alkanethiols by Photoemission Spectroscopies. Figure 2 shows the He-(I) UPS data (kinetic energy scale, 5 V added bias to enhance the detection of the low-KE electrons) for clean gold foils and for gold foils modified with the alkanethiols H_3SH to $H_{18}SH$. Figure 3 shows an expanded view of the Fermi edge region of these photoemission spectra (binding energy scale vs E_F for Au). As the carbon chain length increases, the photoemission spectral features from the underlying gold substrate are replaced at high-KE by the photoionization features of the alkyl chain and at low-KE by an increased intensity in the background of scattered

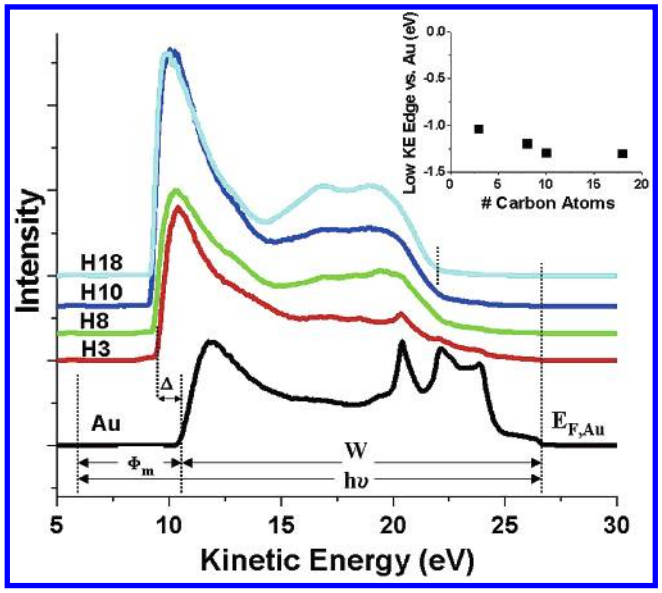

Figure 2. UV photoemission spectra for clean Au and Au modified with H_3SH, H_8SH, $H_{10}SH$, and $H_{18}SH$. The inset shows the shift in the low-KE edge (shift in a vacuum level) of these

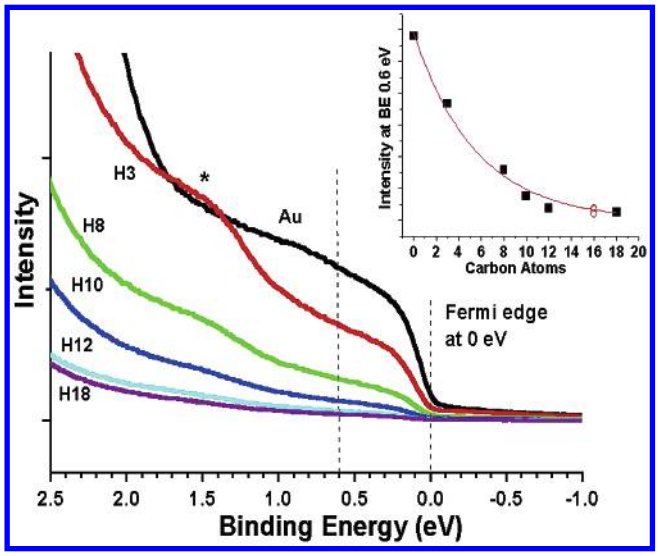

Figure 3. Expanded view of the Au Fermi edge photoemission region for the spectra in Figure 2, showing the systematic loss in intensity of the Au Fermi edge photoemission signal and the growth and loss of a new photoemission feature at ca. 1.4 eV binding energy (*) (3- and 8-carbon chains only). The inset shows the exponential decrease in Au Fermi edge photoemission intensity with increasing alkyl chain length, both for normal alkanes (filled squares) and partially fluorinated alkanes (open circles) chains.

secondary electrons that arose initially from photoemission in the gold near-surface region, as well as in the alkanethiol layer. This background of secondary electrons increases exponentially in intensity to lower kinetic energies and abruptly terminates when the kinetic energy of these secondary electrons no longer exceeds the effective work function of this modified surface. The escape probability for the lowest-KE photoelectrons is strongly sensitive to even small changes in surface composition.[24,49−56]

The photoemission from the Au Fermi edge at higher kinetic energy can be detected above background, even from the surfaces covered with the longest alkyl chains. The residual signal from photoemission from the Au(5d) valence band region (e.g., the spectral feature just above 20 eV KE) is still apparent in the UPS data for H_3SH to H_8SH thin films, but is difficult to resolve above background for the longer chains. The absolute kinetic energy for the gold Fermi edge emission does not shift with increasing carbon chain length, and we assume that electronic equilibrium is maintained between the alkane layers, the gold substrate, and the spectrometer.[22−30] An additional spectral feature is also seen in the UPS data for both H_3SH and H_8SH films on gold, at a binding energy of ca. 1.4 eV (* indicated in the spectra of Figure 3). This is a spectral region where there is no photoemission from the alkane chains and no peak in the Au(5d) photoemission spectrum, and is attributed to ionization of a gold−sulfur orbital.[57−59] From these spectra, and those which follow, the energy of the first ionization potential (IP) is determined with respect to the Fermi energy of the underlying substrate, although these alkanethiols and partially fluorinated alkanethiols provide no fully resolved ionization peak from the HOMO, in contrast to what is often observed for various small molecule adsorbates.[22−30] Shifts in the effective work function (Φ_m) of these modified gold surfaces are monitored by subtracting the width of the He(I) photoemission spectrum (i.e., the difference between the high-KE and low-KE edges of the spectrum (*W*)) from the source energy, 21.2 eV.[22−30] Since the Au Fermi edge feature does not shift with addition of the alkanethiol layer, these changes in Φ_m (Δ—also described as a shift in the vacuum level) are most effectively followed by monitoring changes in the energy of the low-KE edge. In conventional studies of metal and semiconductor surfaces, it is understood that this work function can be altered by the presence of submonolayer organic or inorganic additives that shift the vacuum level at the substrate/adlayer interface, shifting the low-KE edge of the photoemission spectrum by 0.1 to 1.0 eV.[53−56]

The spatial distribution of photoemission events in these alkanethiol layers is important to consider, since shifts in the low-KE edge should sample changes in electronic properties at the gold/SAM interface in order for the calculations of work function changes to be valid. Duwez and co-workers[31,32] and Seki and co-workers[33] have both estimated the escape depth, λ, for photoelectrons at ca. 15 eV kinetic energy (below the Fermi edge photoemission for gold in a He(I) UPS experiment) to be ca. 5−8 Å for compact hydrocarbon monolayer films. Our own data confirm this estimate. The inset in Figure 3 shows that the Fermi edge photoemission intensity decreases exponentially with carbon number in the alkyl chain, and this monotonic decay in Fermi edge intensity with increasing chain length is consistent with the formation of hydrocarbon monolayers that are compact. From this plot, we obtain an inelastic mean free path of ca. 8 Å for escape of photoelectrons through the alkyl chains, at the KE of the Au Fermi edge, assuming an average chain tilt angle of 35°, 1.27 Å incremental chain length per $-CH_2-$ unit, a thickness per $-CH_2-$ unit of $l = 1.27(\cos 35°)$, and a Au−S distance of 2 Å.[34−47] The total sampling depth for the photoemission experiment is conservatively 3λ (i.e., at least 24 Å) near the Au Fermi edge, where the takeoff angle for photoemission is 0° vs the surface normal.[49] The escape depth is further presumed to increase rapidly with decreasing KE below this energy, but with considerable uncertainty in its magnitude,[49−52] and we therefore assume that photoelectrons escaping the alkanethiol layers near the low-KE cutoff, at 0° takeoff angles, sample the entire SAM layer and the gold/SAM interface.

Gas-phase UPS data for H_8SH, $H_{12}SH$, and $H_{18}SH$ are shown in Figure 4a for comparison with the thin-film spectra. It is worth noting when comparing these data to the thin-film UPS data that various conformations of these molecules are likely present

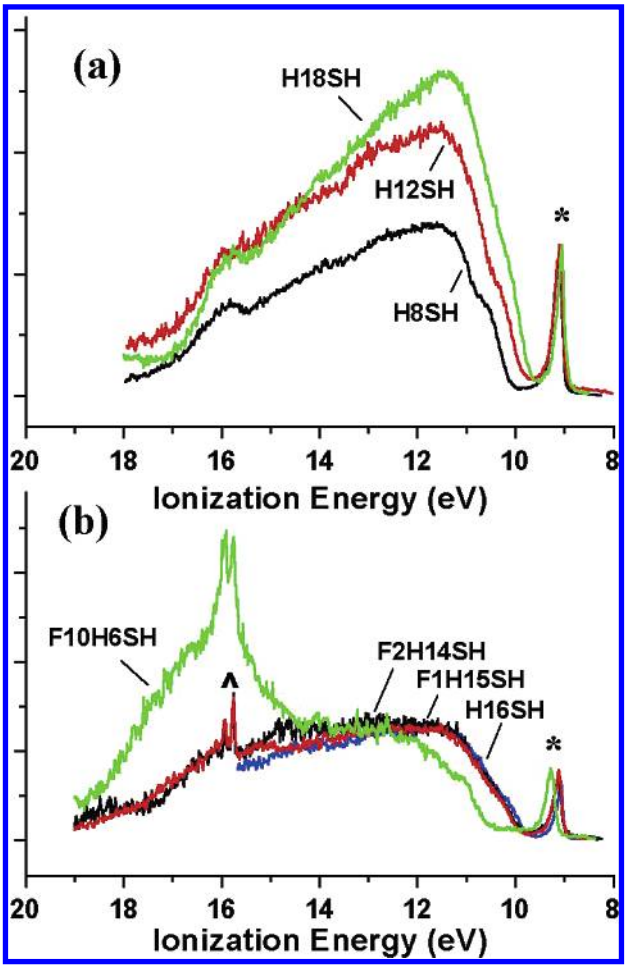

Figure 4. Gas-phase UV photoemission spectra for three different alkanethiols (upper) and three different partially fluorinated alkanethiols (lower). The sharp peak at high KE arises from ionization of the sulfur lone-pair orbitals (marked by (*)). The highest-energy ionization edge for ionization of orbitals of the alkyl chain shift to higher KE with increasing chain length and shift to lower KE with increasing extent of fluorination of the chain (see text). Extra ionizations arising from argon (2p) lines used to calibrate the energy axis are marked with (∧). (See refs 48 and 60.)

in the gas phase, which increases the energy distribution in most spectral features. In the gas-phase spectra the alkyl C−C and C−H σ-bond ionizations fall under the featureless ionization band from ca. 10−17 eV. The thiol S−H σ-bond ionization should also occur in this region, but is not clearly resolved. For these gas-phase spectra, the low ionization energy edge of the alkyl band decreases as the length of the alkyl chain increases. Photoemission spectra for the thin films from eight-carbon and longer alkyl chains (Figure 2) show an onset for the alkyl chain ionizations at about 8 eV, which is lower by another ca. 1.0 eV than that which is observed in the gas-phase photoelectron spectra of the longest alkyl chains. This additional stabilization can be attributed to photoionization in a condensed phase environment and the polarization of that environment to screen the core−hole charge created in the photoemission event.[49] The gas-phase spectra also show an additional ionization feature (* in Figure 4a and Figure 4b) that is due to the ionization of a sulfur 3p lone pair orbital, which does not shift appreciably with increasing alkyl chain length.[31−32]

Figure 5 shows a series of UV-photoemission spectra taken from Au surfaces modified with either the $H_{16}SH$ or with the mono-, di-, tetra-, and decafluoro-substituted versions of this same alkanethiol ($F_1H_{15}SH$, $F_2H_{14}SH$, $F_4H_{12}SH$, and $F_{10}H_6SH$,

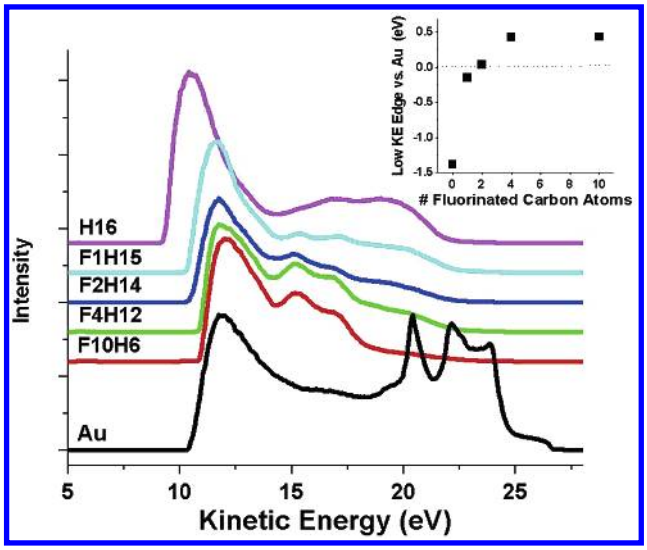

Figure 5. UV photoemission spectra for clean Au and Au modified with C_{16}-alkane thiols, fluorinated at the outer 1, 2, 4, and 10 methylene positions (F_yH_xSH; $y = 0$, $x = 16$, $y = 1$, $x = 15$; $y = 2$, $x = 14$; $y = 4$, $x = 12$; $y = 10$, $x = 6$). The inset shows the shift in the low-KE cutoff energy as a function of the number of fluorinated methylene units, relative to the low-KE cutoff energy for clean Au. The addition of one CF_3 group at the terminus of the alkyl chain is nearly sufficient to increase the low-KE cutoff to that for clean Au, additional fluorination of the chain makes the effective work function exceed that of clean Au.

respectively). Despite the fact that these chains are expected to exhibit slightly less dense packing and larger effective thickness as the extent of fluorination increases,[36−44] the attenuation of the Au Fermi edge signal is consistent for all of the fluorinated alkyl chains examined, and scales with the number of carbons in the alkyl chain, as seen with the normal alkyl chains (see open circles in inset of Figure 3). As the extent of fluorination increases at the chain terminus, there is a systematic increase in the low-KE cutoff energy of these photoemission spectra. The difference in low-KE edge between the $H_{16}SH$- and F_4H_{12}-SH-modified Au surfaces is ca. 1.8 eV (inset in Figure 5), consistent with addition to the Au surface of a large interfacial dipole of opposite sign to that observed for the alkyl chains alone (see below).

The gas-phase photoemission data for three of the partially fluorinated chains (Figure 4b) demonstrate the changes in the photoemission band features as the degree of fluorination increases. These changes include an increase in intensity in the high-ionization-energy region of the spectra due to the addition of ionizations from fluorine lone pairs and C−F σ-bonds, the decrease in intensity of the spectral features in the low ionization energy region of the spectra due to the removal of C−H σ-bonds, and an increase in ionization energy edge associated with C−H and C−C σ-bonds as electron-withdrawing fluorine atoms are added in adjacent regions of the alkane chain. In the partially fluorinated alkyl chains, the ionization energy from the sulfur 3p lone pair increases as well. From these data, we estimate the differences in onset for ionization of the alkyl and partially fluorinated alkyl chains to be ca. 4.6 eV, a difference which is sustained in the UPS data of the thin films of these molecules (see further discussion below and Table 1).

We also observed that the shift in the low-KE edge for photoemission from the partially fluorinated alkanethiols was dependent upon the orientation of the terminal-CF_3 group. Figure 6 shows the UPS data for a series of alkanethiol chains, fluorinated only at the terminus of each chain, $F_1H_{12-15}SH$, where it can be observed that the low-KE cutoff energy for these

TABLE 1: Ionization Potentials from Gas-Phase Photoelectron Spectroscopy of Thiols

thiol	IP, sulfur lone pair (eV) ±0.02	IP, alkyl orbitals (eV) ±0.02	Δ S−alkyl (eV) ± 0.04
H8	9.09	10.07	0.98
H12	9.09	9.79	0.70
H18	9.06	9.59	0.53
F1H15	9.12	9.82	0.70
F2H14	9.12	9.87	0.74
F10H2	9.68	11.24	1.56
F10H6	9.27	10.47	1.20

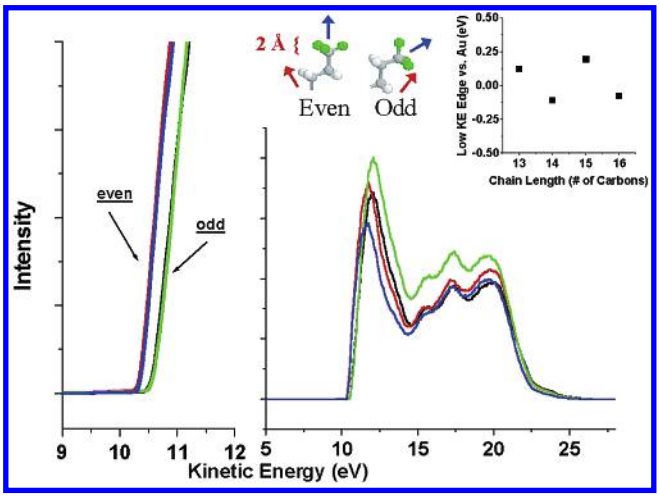

Figure 6. UV photoemission spectra for a series of alkanethiols on Au having a single CF_3 termination with either odd or even numbers of carbon atoms in the alkyl chain. The low-KE edge region has been expanded to show the difference in the energy of this edge for even- and odd-numbered carbon chains. Inset (upper left) is a schematic of how the orientation of the terminal methyl group of an alkanethiol changes when the total number of carbons is even or odd. In this schematic, the surface is horizontal below the models, the red arrow (adjacent to the molecule) represents the direction of the total dipole moment for the entire alkane chain, and the blue arrow (above the molecule) represents the dipole moment from just the terminal groups. Inset (upper right) shows the low-KE cutoff energy as a function of carbon chain length, confirming this "odd/even effect" in the interface dipole.

photoemission spectra is greater for odd chain lengths than for even chain lengths (by ca. 0.3 eV). Previous studies of F_1H_X alkanethiols have shown that the orientation of the terminal CF_3-groups changes significantly depending upon whether the total number of carbon atoms in the chain is even or odd, and this affects some physical properties, such as wettability and probe ion neutralization probabilities.[20,21,44] (See further discussion below.)

Estimation of Interface Dipoles from Molecular Orbital Calculations. Changes in metal surface potentials accompanying adsorption of an alkanethiol monolayer have been described by eq 1, assuming that the dipoles in the monolayer are well ordered with respect to the surface:

$$\Delta U = N(\mu_{\mathrm{mol},\perp}/\epsilon - \mu_{\mathrm{Au-S}}) \quad (1)$$

where ΔU is the change in surface potential (shift in a vacuum level) with surface modification upon adsorption of the alkanethiol layer, N is the areal density of molecules, $\mu_{\mathrm{mol},\perp}$ is the dipole moment of an individual molecule in the thin film projected onto the axis normal to the surface, $\mu_{\mathrm{Au-S}}$ is the intrinsic dipole moment of the gold−sulfur bond, and ϵ is the static dielectric constant of the molecular layer.[2] For self-assembled monolayers of alkanethiols on gold, N is ca. (3−5) $\times$ 10^{14} cm^{-2}, and ϵ is estimated between 2 and 3.[1−4,12,15−18] All of the monolayers in the studies reported here are expected to have similar gold−sulfur interactions and packing densities.[39] We therefore calculated dipole moments of the individual alkanethiols and used these as an estimate of the sum of molecular dipoles expressed within the SAM films. All computations were performed using Gaussian 98.[61] The geometry of the free thiol was optimized with a basic STO-3G ab initio basis set (starting from an all-trans geometry), then the thiol hydrogen was removed, and the dipole moment of the neutral radical was calculated at the unrestricted Hartree−Fock level with the more comprehensive 6-31+G ab initio basis set.[2,5] The neutral radical was used because the thiol hydrogen is known to dissociate in the formation of a self-assembled monolayer; however, the exact state of the charge distribution in the gold−sulfur bond is still debated (see below).[18,62,63] We follow the convention in which the dipole vector is presumed to point *toward* the negative pole, the calculated dipole vectors therefore point primarily toward the sulfur atom for hydrocarbon alkane thiols. (See Figure 1b for an illustration of selected molecules with total calculated dipole vector and dipole vectors projected along the molecular axis).

The resultant calculated molecular dipole moments are oriented at varying angles relative to the central axis of the alkyl chain; therefore, for comparison purposes, we also calculated the projection of these dipoles along the molecular axis and along the surface normal axis, which are the two most critical directions to consider for photoelectrons escaping through these thin films.[2,5] The molecular axis is defined as a linear least-squares fit of the position of all of the carbons in the alkanethiol backbone. The projection of the dipole along the surface normal axis was calculated assuming a ($\sqrt{3}$ tme $\sqrt{3}$)R30° packing structure and an sp^3 binding mode for sulfur (such that the surface−S−C bond angle of is approximately 104°) without a larger "super-cell" arrangement.[61,64,65] For all systems, a tilt angle of 35° and a β-twist angle of 55° (rotation around the molecular axis) was assumed.[1,32,43,62−65] These assumptions greatly simplify the comparisons between alkanethiol layers to follow, and are compatible with a semiquantitative interpretation of the origin of the interface dipole effects. As summarized in Figure 1, SAMs on gold with more than four terminally fluorinated carbon atoms are believed to become less tilted in the fluorinated regions of the chain, nevertheless, we estimated that these changes in tilt angle would introduce errors in projected dipole moments of less than 10−20% and therefore ignore this factor for the comparisons to follow. All computational results are summarized in Table 2.

Figure 7a shows that the shift in a vacuum level versus clean Au varies slightly with molecular dipole moment (projected along the surface normal) and with hydrocarbon chain length (see also the inset in Figure 2). As noted in previous studies,[2] the dipole moment is rather insensitive to the number of carbons in the chain, changing by less than 0.1 D as the chain grows from H_3SH to $H_{18}SH$. The calculated dipole moment in these molecules is dominated by the electron-rich sulfur terminus. The surface potential shifts with alkyl chain length 19 mV/CH_2 unit (from a fit of potential shift versus carbon number for all hydrocarbon alkanethiol SAMs measured). Previous Kelvin probe studies have produced slopes in similar plots of 9.3 mV/CH_2 unit; 14.1 mV/CH_2 unit; and 20 mV/CH_2 unit for alkanethiol monolayers on gold.[2,15,19]

TABLE 2: Shifts in Effective Work Function and Calculated Dipole Moments for Alkanethiol and Partially Fluorinated Alkanethiol Monolayers on Au

SAM-modified surface	molecular formula Au (sputtered)	low-KE cutoff (eV)[a] ±0.05	shift in effective vacuum level (eV)[b] ± 0.1	total dipole (D)[c]	angle: dipole-to-molecule (°)[d]	dipole along molecular axis (D)[e]	dipole along normal axis (D)[f]
Au		10.45	0.00				
H3	$HS(CH_2)_2CH_3$	9.44	−1.01	2.29	24	2.1	1.4
H8	$HS(CH_2)_7CH_3$	9.28	−1.17	2.48	27	2.2	1.5
H10	$HS(CH_2)_9CH_3$	9.18	−1.27	2.50	28	2.2	1.4
H18	$HS(CH_2)_{17}CH_3$	9.17	−1.28	2.51	27	2.2	1.5
H16	$HS(CH_2)_{15}CH_3$	9.10	−1.35	2.51	26	2.3	1.5
F1H15	$HS(CH_2)_{15}CF_3$	10.33	−0.12	−2.91	−67	−1.2	−1.8
F2H14	$HS(CH_2)_{14}(CF_2)CF_3$	10.51	0.06	−1.50	9	−1.5	−1.1
F4H12	$HS(CH_2)_{12}(CF_2)_3CF_3$	10.90	0.45	−1.79	7	−1.8	−1.4
F10H6	$HS(CH_2)_6(CF_2)_9CF_3$	10.91	0.46	−1.94	7	−1.9	−1.5
F1H12	$HS(CH_2)_{12}CF_3$	10.57	0.12	−1.25	25	−1.1	−0.7
F1H13	$HS(CH_2)_{13}CF_3$	10.34	−0.11	−2.91	−67	−1.1	−1.8
F1H14	$HS(CH_2)_{14}CF_3$	10.64	0.19	−1.25	26	−1.1	−0.7
F1H15	$HS(CH_2)_{15}CF_3$	10.33	−0.12	−2.91	−67	−1.1	−1.8

[a] Low-KE edge of the photoemission spectrum, measured as the tangent to the low-KE side of the spectrum.[23,25] [b] Shift of low-KE cutoff vs low-KE cutoff of clean gold, providing an indication of the change in a vacuum level.[22−30] [c] Magnitude of calculated dipole, neutral radical calculated with Gaussian UHF/6-31+G basis set (see text). [d] Angle between the calculated dipole and the molecular axis. [e] Magnitude of the calculated dipole projected along the molecular axis. [f] Magnitude of the calculated dipole projected normal to the Au surface—assuming 35 degree tilt angle and 55 degree β tilt (see text).

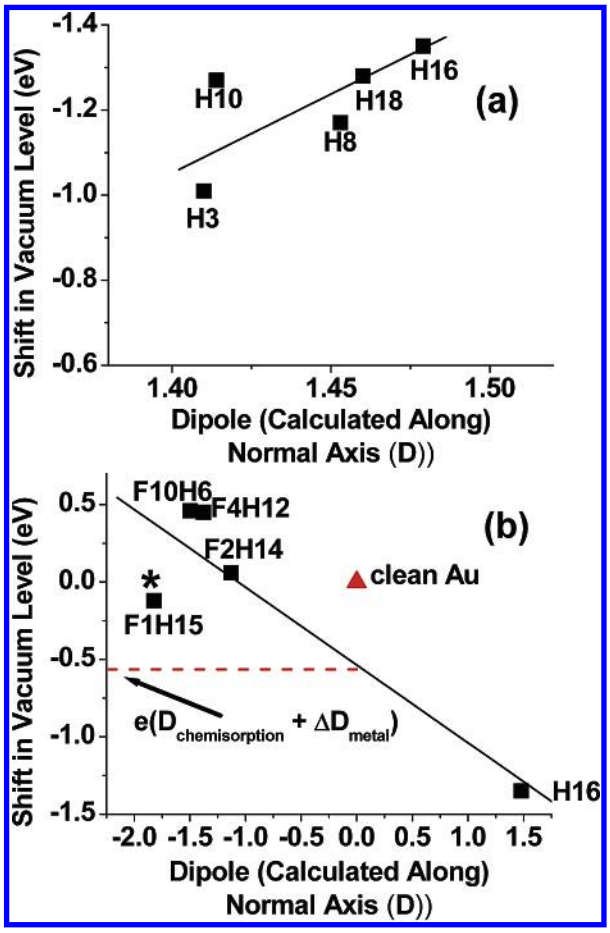

Figure 7. Shift in effective vacuum level (vs clean Au) versus the calculated dipole moment (projected along the normal axis) for alkanethiol and partially fluorinated alkanethiol monolayers on Au. (a) Normal alkanethiols, H_3−H_{18}, increasing chain length from left to right (see Table 2 for values). (b) Partially fluorinated alkanethiols (entire series from $F_{10}H_6$ to H_{16}). The star symbol (*) indicates F_1H_{15}, and the triangle indicates the reference level for clean Au.

Figure 7b plots the shift in a vacuum level versus the calculated normal axis dipole moment for the partially fluorinated alkane thiol series ($F_1H_{15}SH$, $F_2H_{14}SH$, $F_4H_{12}SH$, and $F_{10}H_6SH$) and for $H_{16}SH$. Because it lies outside the correlation line, the data for $F_1H_{15}SH$ are marked with a (*). Clean gold is represented by the red triangle at (0,0). The molecules chosen for this plot have the same length (16 carbons total in each molecule) while the calculated dipole moment varies significantly with fluorination, ranging from $H_{16}SH$ (1.5 normal, 2.3 D along molecule) to $F_{10}H_6SH$ (−1.5 D normal, −1.9 D along molecule). The larger variation in dipole moment for this series of molecules allows a more substantive comparison with eq 1 than does the plot in Figure 7a. With the exception of F_1H_{15}-SH, the vacuum level shift appears to correlate reasonably well with the calculated dipole moment. A least-squares fit of these data gives a *y*-intercept of ca. −0.5 eV.

The confidence in this plot would improve with consideration of vacuum level shifts for SAM layers with smaller positive or negative dipole moments than the simple alkanes, or semi-fluorinated alkanes, considered here. Shifts in vacuum levels caused by addition of phenyl-terminated H12 and H13 alkanethiols are currently under exploration in our group, the details of which will be communicated shortly. It can be said at present, however, that the addition of a phenyl group to the alkane chain produces a molecule with a smaller positive dipole moment than seen for the methyl-terminated chain. The vacuum level shift decreases from the methyl-terminated SAMs to the phenyl-terminated SAMs, correlating well with the dipole moment change and suggesting that the trend contained in Figure 7b will be supported as additional self-assembled monolayers are measured.

The change in surface potential for adsorption of a molecular layer on a clean metal has been generally approximated as a series of linearly additive contributions:

$$\Delta U = (U_{\text{metal+monolayer}} - U_{\text{cleanmetal}}) = eD_{\text{chemisorption}} + eD_{\text{molecule}} + \Delta eD_{\text{metal}} \quad (2)$$

$D_{\text{chemisorption}}$ in eq 2 is the dipole moment introduced by charge-transfer based on bond formation during chemisorption (e.g., the formation of the gold−thiolate bond); D_{molecule} is the intrinsic dipole moment of the adsorbate (i.e., the dipole moment of the

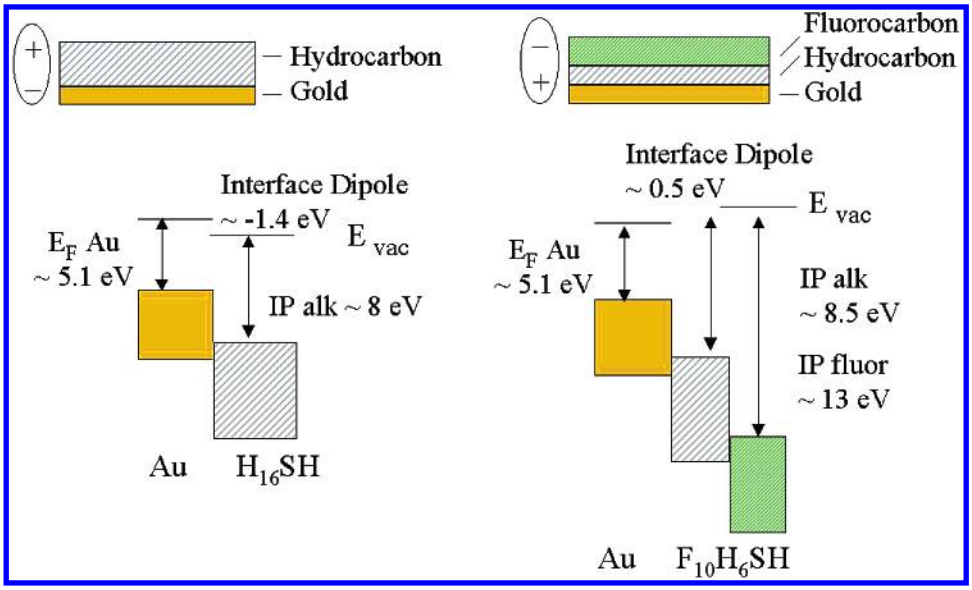

Figure 8. Schematic view of the band-edge offsets for Au modified with normal alkanethiols (left) and Au modified with a typical partially fluorinated alkanethiol (right). The maximal magnitude and signs of the interface dipoles are shown, along with the approximate positions of the ionization edges for each portion of the chain.

alkyl or partially fluorinated alkyl chain); ΔeD_{metal} represents the change in metal surface potential due to addition of *any* adsorbate, which generally is large and positive and varies with the nature of the metal but not significantly with the identity of the molecular overlayer.[13,66] Crispin et al. have recently reviewed the literature available to estimate values of ΔeD_{metal} and have shown that the change in surface potential of a clean metal during simple physisorption of a noninteracting species, such as Xe atoms, can be approximately linearly correlated with the intrinsic metal surface dipole:

$$\Delta U_{metal}\,(\Delta eD_{metal}) \approx 0.2 eD_{metal} \qquad (3)$$

where D_{metal} is the intrinsic surface dipole.[13] Shifts in work function of ca. 0.1 eV to 1.0 eV, as measured from photoemission spectra of adsorbed Xe on clean metals (PAX) have been observed for metal surface dipole fields (eD) ranging from 0.1 to 5.5 eV. There are only two studies that we are aware of for photoemission of Xe adsorbed on clean Au surfaces (Au⟨100⟩ and polycrystalline Au), and estimates of a decrease in work function of ca. 0.45 to 0.52 eV have been determined for these two surfaces.[67,68] These measurements provide us with an estimate of ΔeD_{metal} due to the addition of any adsorbate to gold, including the alkanethiol layer.

We assume that the Au−S interaction is similar for all of the molecules reported here and that the change in metal surface dipole due to the presence of these adsorbates should also be comparable for all molecules explored. The *y*-intercept of the plot of ΔU vs $D_{molecule}$ in Figure 7b represents the change in surface potential due to chemisorption and physisorption: $eD_{chemisorption} + \Delta eD_{metal}$ = ca. −0.5 eV. From the difference between this intercept and the estimate for ΔeD_{metal} from PAX measurements on gold, we estimate that the surface potential shift due to the Au−S interaction is small, between +0.02 eV and −0.05 eV. If surface potential shifts on gold due to physisorption were greater than ca. 0.5 eV, our estimated magnitude for $eD_{chemisorption}$ would increase, consistent with a larger dipole moment in the gold−thiolate bond.[1−5,19] From the Kelvin probe and PES data collected to date, however, it appears that the Au−S bond does not have as large a dipole as would be expected for a sulfur−metal interaction involving appreciable charge transfer. There are, in addition, several recent reports which suggest that a covalent Au−S bond with a small intrinsic dipole is a more appropriate description for these self-assembled monolayers.[12,18,69]

The observed changes in photoemission spectra for CF_3-terminated SAMs of even or odd chain length (Figure 6) are interesting. Odd-numbered alkyl chains produce surfaces with higher effective work functions than even-numbered alkyl chains—a trend that is not predicted by the net dipole moments calculated either along the molecular axis or surface normal (Table 2). As shown in the inset schematic of Figure 6, we can best rationalize the UPS results if the dipole along the *most exposed* C−F bond(s) dominates the probability for escape of the low-KE photoelectrons. This is consistent with our other findings that the shift of the low-KE edge in the semi-fluorinated alkanethiols is mainly influenced by the functional group at the thin film/vacuum interface.

Experiments involving ion neutralization on these same surfaces, where a 20−30 eV probe ion (such as $C_6H_6^+$, or $C_4H_4N_2^+$) collides with the SAM-modified Au substrate show a similar odd−even effect.[21] The yield of neutral benzene or pyrazine after such collisions is extremely sensitive to the composition and effective work function of the outermost regions of these thin films, and the neutralization probabilities are in general lower for odd- versus even-carbon-chain-length SAMs, consistent with the higher effective work functions for such surfaces. Apparently the dipolar fields which influence the low-KE cutoff energy in the photoemission experiments also are most important in controlling electron injection into molecular probe ions.

Numerous wettability studies of CF_3-terminated SAMs, which also exhibit systematic "odd-even" effects,[35−40] however, have shown that CF_3-terminated SAMs having even numbers of carbon atoms are more wettable by polar liquids than are their counterparts having odd numbers of carbon atoms. This trend in wettability *does* show a good correlation with dipole computed normal to the substrate (Table 2). The apparent conflicts in these studies suggest that UV-photoemission and ion−neutralization studies may be influenced by somewhat different electrostatic factors than wettability by polar liquids, and that surface dipole fields may influence the escape of low-

KE photoelectrons from a CF_3-terminated alkane chain differently than polar liquid wettability.

Conclusions

Figure 8 shows a schematic view of the band-edge offsets for alkanethiol and partially fluorinated alkanethiol monolayers on gold, and cross-section schematics of these thin films, drawn as heterojunctions for $H_{16}SH$ and $F_{10}H_6SH$. We use the IP and low-KE cutoff values from Figures 2 and 5, Tables 1 and 2, and the gas-phase photoemission data to predict the differences in IP for the normal and fluorinated regions of these chains and to estimate shifts in a vacuum level at the metal/SAM interface. For this figure we chose the 16-carbon chain systems with fluorination of 10 methylene units, to show the greatest difference between frontier orbital position between normal and fluorinated regions of the alkyl chain. Clearly as such alkyl chains are functionalized with electron-donating or electron-withdrawing substituents, we expect to be able to vary the vacuum level and effective work function of a gold contact over a span of ca. 2 eV, as has been previously demonstrated for other alkanethiol surface modifiers.[2−5,15] It is now of interest to systematically extend these studies to molecular systems capable of forming true covalent interactions with the metal or semiconductor surface, and to modifiers which are aromatic or partially aromatic in character, where charge injection need not occur exclusively through tunneling through a nonconductive hydrocarbon layer.

Acknowledgment. We gratefully acknowledge support for this research from the National Science Foundation (CHE-9732650, CHE-0211900), and the NSF-Center for Materials and Devices for Information Technology−DMR-0120967 (N.R.A.), CHE-9224719 to VW, and DMR-9700662 to T.R.L.), the Materials Characterization Program at the University of Arizona, and the Alexander von Humboldt Stiftung Forschungspreis (N.R.A.). T.R.L. acknowledges additional support from the Robert A. Welch Foundation (E-1320) and the Texas Advanced Research Program (003652-0307-2001). M.H. thanks the German ZAP (Zentrum für Angewandte Photonik, Center of Applied Photonics) for financial support. We also gratefully acknowledge recent discussions with Xavier Crispin and Jean-Luc Brédas.

Supporting Information Available: Detailed X-ray photoelectron spectroscopic characterization of the partially fluorinated thin films. This material is available free of charge via the Internet at http://acs.org.

References and Notes

(1) Ulman, A. *Chem. Rev.* **1996**, *96*, 1533−1554.
(2) Evans, S. D.; Ulman A. *Chem. Phys. Lett.* **1990**, *170*, 462−466.
(3) Campbell, I. H.; Kress, J. D.; Martin, R. L.; Smith, D. L.; Barashkov, N. N.; Ferraris, J. P. *Appl. Phys. Lett.* **1997**, *71*, 3528−3530.
(4) Campbell, I. H.; Rubin, S.; Zawodzinski, T. A.; Kress, J. D.; Martin, R. L.; Smith, D. L.; Barashkov, N. N.; Ferraris, J. P. *Phys. Rev. B* **1996**, *54*, 14321−14324.
(5) Zehner, R. W.; Parsons, B. F.; Hsung, R. P.; Sita, L. R. *Langmuir* **1999**, *15*, 1121−1127.
(6) Wold, D. J.; Frisbie, C. D. *J. Am. Chem. Soc.* **2001**, *123*, 5549−5556.
(7) Chabinyc, M. L.; Chen, X. X.; Holmlin, R. E.; Jacobs, H.; Skulason, H.; Frisbie, C. D.; Mujica, V.; Ratner, M. A.; Rampi, M. A.; Whitesides, G. M. *J. Am. Chem. Soc.* **2002**, *124*, 11730−11736.
(8) Beebe, J. M.; Engelkes, V. B.; Miller, L. L.; Frisbie, C. D. *J. Am. Chem. Soc.* **2002**, *124*, 11268−11269.
(9) Bastide, S.; Butruille, R.; Cahen, D.; Dutta, A.; Libman, J.; Shanzer, A.; Sun, L. M.; Vilan, A. *J. Phys. Chem. B* **1997**, *101*, 2678−2684.
(10) Vilan, A.; Shanzer, A.; Cahen, D. *Nature* **2000**, *404*, 166−168.
(11) Ashkenasy, G.; Cahen, D.; Cohen, R.; Shanzer, A.; Vilan, A. *Acc. Chem. Res.* **2002**, *35*, 121−128.
(12) Bruening, M.; Cohen, R.; Guillemoles, J. F.; Moav, T.; Libman, J.; Shanzer, A.; Cahen, D. *J. Am. Chem. Soc.* **1997**, *119*, 5720−5728.
(13) Crispin, X.; Geskin, V.; Crispin, A.; Cornil, J.; Lazzaroni, R.; Salaneck, W. R.; Bredas, J. L. *J. Am. Chem. Soc.* **2002**, *124*, 8131−8141.
(14) Bruner, E. L.; Koch, N.; Span, A. R.; Bernasek, S. L.; Kahn, A.; Schwartz, J. *J. Am. Chem. Soc.* **2002**, *124*, 3192−3193.
(15) Lü, J.; Delamarche, E.; Eng, L.; Bennewitz, R.; Meyer, E.; Güntherodt, H.-J. *Langmuir* **1999**, *15*, 8184−8188.
(16) Pflaum, J.; Bracco, G.; Schreiber, F.; Colorado, R., Jr.; Shmakova, O. E.; Lee, T. R.; Scoles, G.; Kahn, A. *Surf. Sci.* **2002**, *498*, 89−104.
(17) Donhauser, Z. J.; Mantooth, B. A.; Kelly, K. F.; Bumm, L. A.; Monnell, J. D.; Stapleton, J. J.; Price, D. W.; Rawlett, A. M.; Allara, D. L.; Tour, J. M.; Weiss, P. S. *Science* **2001**, *292*, 2303−2307.
(18) Howell, S.; Kuila, D.; Kasibhatla, B.; Kubiak, C. P.; Janes, D.; Reifenberger, R. *Langmuir* **2002**, *18*, 5120−5125.
(19) Ratner, M. *Nature* **2000**, *404* (6774), 137−138.
(20) Smith, D. L.; Wysocki, V. H.; Colorado, R.; Shmakova, O. E.; Graupe, M.; Lee, T. R. *Langmuir* **2002**, *18*, 3895−3902.
(21) Angelico, V. J.; Mitchell, S. A.; Wysocki, V. H. *Anal. Chem.* **2000**, *72*, 2603−2608.
(22) Seki, K.; Hayashi, N.; Oji, H.; Ito, E.; Ouchi, Y.; Ishii, H. *Thin Solid Films* **2001**, *393*, 298−303.
(23) Ishii, H.; Sugiyama, K.; Ito, E.; Seki, K. *Adv. Mater.* **1999**, *11*, 605−625.
(24) Cahen, D.; Kahn, A. *Adv. Mater.* **2003**, *15*, 271−277.
(25) Schlaf, R.; Parkinson, B. A.; Lee, P. A.; Nebesny, K. W.; Armstrong, N. R. *J. Phys. Chem. B* **1999**, *103*, 2984−2992.
(26) Schlettwein, D.; Hesse, K.; Gruhn, N. E.; Lee, P. A.; Nebesny, K. W.; Armstrong, N. R. *J. Phys. Chem.* **2001**, *105*, 4791−4800.
(27) Blochwitz, J.; Fritz, T.; Pfeiffer, M.; Leo, K.; Alloway, D. M.; Lee, P. A.; Armstrong, N. R. *Org. Electronics* **2001**, *2*, 97−104.
(28) Greczynski, G.; Kugler, T.; Salaneck, W. R. *J. Appl. Phys.* **2000**, *88*, 7187−7191.
(29) Fahlman, W.; Salaneck, W. R. *Surf. Sci.* **2002**, *500*, 904−922.
(30) Koch, N.; Kahn, A.; Ghijsen, J.; Pieraux J.-J.; Schwartz, J.; Johnson, R. L.; Eischner, A. *Appl. Phys. Lett.* **2003**, *82*, 70−72.
(31) Duwez, A. S.; DiPaolo, S.; Ghijsen, J.; Riga, J.; Deleuze, M.; Delhalle, J. *J. Phys. Chem. B* **1997**, *101*, 884−890.
(32) Duwez, A. S; Pfister-Guillouzo, G.; Delhalle, J.; Riga, J. *J. Phys. Chem. B* **2000**, *104*, 9029−9037.
(33) Seki, K.; Ueno, N.; Karlsson, U. O.; Engelhardt, R.; Koch, E.-E. *Chem. Phys.* **1986**, *105*, 247−265.
(34) Nuzzo, R. G.; Dubois, L. H.; Allara, D. L. *J. Am. Chem. Soc.* **1990**, *112*, 558−569.
(35) Miura, Y. F.; Takenaga, M.; Koini, T.; Graupe, M.; Garg, N.; Graham, R. L., Jr.; Lee, T. R. *Langmuir* **1998**, *14*, 5821−5825.
(36) Graupe, M.; Takenaga, M.; Koini, T.; Colorado, R., Jr.; Lee, T. R. *J. Am. Chem. Soc.* **1999**, *121*, 3222−3223.
(37) Colorado, R., Jr.; Graupe, M.; Takenaga, M.; Koini, T.; Lee, T. R. *Mater. Res. Soc. Symp. Proc.* **1999**, *546*, 237−242.
(38) Colorado, R., Jr.; Lee, T. R. *J. Phys. Org. Chem.* **2000**, *13*, 796−807.
(39) Colorado, R., Jr.; Graupe, M.; Kim, H. I.; Takenaga, M.; Oloba, O.; Lee, S.; Perry, S. S.; Lee, T. R. In *Interfacial Properties on the Submicron Scale*; Frommer, J. E., Overney, R., Eds.; ACS Symposium Series 781; American Chemical Society: Washington, DC, 2001; pp 58−75.
(40) Colorado, R., Jr.; Lee, T. R. *Langmuir* **2003**, *19*, 3288−3296.
(41) Kim, H. I.; Koini, T.; Lee, T. R.; Perry, S. S. *Langmuir* **1997**, *13*, 7192−7196.
(42) Houssiau, L.; Graupe, M.; Colorado, R.; Kim, H. I.; Lee, T. R.; Perry, S. S.; Rabalais, J. W. *J. Chem. Phys.* **1998**, *109*, 9134−9147.
(43) Tamada, K.; Ishida, T.; Knoll, W.; Fukushima, H.; Colorado, R.; Graupe, M.; Shmakova, O. E.; Lee, T. R. *Langmuir* **2001**, *17*, 1913−1921.
(44) Frey, S.; Heister. K.; Zharnikov. M.; Grunze, M.; Tamada, K.; Colorado, R.; Graupe, M.; Shmakova, O. E.; Lee, T. R. *Israel J. Chem.* **2000**, *40*, 81−97.
(45) Graupe, M.; Koini, T.; Wang V. Y.; Nassif, G. M.; Colorado, R., Jr.; Villazana, R. J.; Dong, H.; Miura, Y. F.; Shmakova, O. E.; Lee, T. R. *J. Fluorine Chem.* **1999**, *93*, 107.
(46) Wagner, A. J.; Han, K. P.; Vaught, A. L.; Fairbrother, D. H. *J. Phys. Chem B* **2000**, *104*, 3291−3297.
(47) Heister, K.; Zharnikov, M.; Grunze, M.; Johansson, L. S. O.; Ulman, A. *Langmuir* **2001**, *17*, 8−11.
(48) Gruhn, N. E.; Lichtenberger, D. L.; Ogura, H.; Walker, F. A. *Inorg. Chem.* **1999**, *38*, 4023.
(49) Cardona, M.; Ley, L., Eds. *Photoemission in Solids I*; Springer-Verlag: New York, 1978.
(50) Klekamp, A.; Umbach, E. *Surf. Interface Anal.* **1992**, *18*, 439−442.

(51) Li, X.; Zhang, Z.; Heinrich, V. E. *J. Electron Spectrosc. Relat. Phenom.* **1993**, *63*, 253−265.
(52) Powell, C. J.; Jablonski, A.; Tilinin, I. S.; Tanuma, S.; Penn, D. R. *J. Electron. Spectrosc. Relat. Phenom.* **1999**, *99*, 1−15.
(53) Brillson, L. J. *Surf. Sci.* **1994**, *299/300*, 909−927.
(54) Wandelt, K.; Hulse, J. E. *J. Chem. Phys.* **1984**, *80*, 1340.
(55) Wandelt, K. *Appl. Surf. Sci.* **1997**, *111*, 1−10.
(56) Horn, K. *Appl. Surf. Sci.* **2000**, *166*, 1−11.
(57) Nyberg, G. L.; Anderson, S. E. *J. Electron. Spectrosc. Relat. Phenom.* **1990**, *52*, 735−746.
(58) Kera, S.; Setyoyama, H.; Kimure, K.; Iwasaki, A.; Okudaira, K. K.; Harada, Y.; Ueno, N. *Surf. Sci.* **2001**, *482−485*, 1192−1198.
(59) Whelan, C. M.; Barnes, C. J.; Walker, C. G. H.; Brown, N. M. D. *Surf. Sci.* **1999**, *425*, 195−211.
(60) Kimura, K.; Katasumata, S.; Achiba,Y.; Yamazaki, T.; Iwata, S. *Handbook of HeI Photoelectron Spectra of Fundamental Organic Molecules;* Halsted Press: New York, 1981.
(61) Gaussian 98, Revision A.11.1, Gaussian, Inc. Pittsburgh, PA, 2001.
(62) Krüger, D.; Fuchs, H.; Rousseau, R.; Marx, D.; Parrinello, M. *J. Chem. Phys.* **2001**, *115*, 4776−4786.
(63) Sellers, H.; Ulman, A.; Shnidman, Y.; Eilers, J. E. *J. Am. Chem. Soc.* **1993**, *115*, 9389−9401.
(64) Zeng, C. G.; Li, B.; Wang, B.; Wang, H. Q.; Wang, K. D.; Yang, J. L.; Hou, J. G.; Zhu, Q. S. *J. Chem. Phys.* **2002**, *117*, 851−856.
(65) Li, T.-W.; Chao, I.; Tao, Y.-Y. *J. Phys. Chem. B* **1998**, *102*, 2935−2946.
(66) Peisert, H.; Knupfer, M.; Fink, J. *Appl. Phys. Lett.* **2002**, *81*, 2400−2402.
(67) McElhiney, G.; Pritchard, J. *Surf. Sci.* **1976**, *60*, 397−410.
(68) Ishi, S.; Viswanathan, B. *Thin Solid Films* **1991**, *201*, 373−402.
(69) Rodriguez, J. A.; Dvorak, J.; Jirsak, T.; Liu, G.; Hrbek, J.; Aray, Y.; Gonzalez, C. *J. Am. Chem. Soc.* **2003**, *125*, 276−285.